Chemical Science

Accepted Manuscript

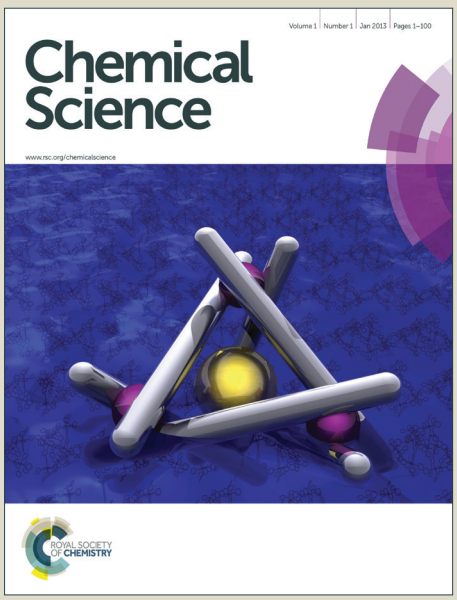

ROYAL SOCIETY OF CHEMISTRY

www.rsc.org/chemicalscience

Journal Name

ARTICLE

Self-Complementary Double-Stranded Porphyrin Arrays Assembled from an Alternating Pyridyl–Porphyrin Sequence

Received 00th January 20xx,
Accepted 00th January 20xx

DOI: 10.1039/x0xx00000x

www.rsc.org/

Mitsuhiko Morisue,*[a] Yuki Hoshino,[a] Kohei Shimizu,[a] Masaki Shimizu[a] and Yasuhisa Kuroda[a]

Oligomeric porphyrin arrays with an alternating pyridyl–porphyrin sequence were synthesized to explore double-strand formation through self-complementary pyridyl-to-zinc axial coordination bonds. Competitive titration experiments revealed the thermodynamic aspects involved in the zipper effect within double-strand formation. Multiple axial coordination bonds defined the stacked conformation, despite a marginal contribution to the stability of the double-strands. Thus, zipper cooperativity was the dominant factor in the remarkable stability. Moreover, the dimeric and trimeric porphyrin arrays were independently assembled into the double-strands by self-sorting from a binary mixture. Double-strand formation engineered the discretely stacked π-system. Successive slipped-cofacial stacks of the porphyrin rings progressively extended the π-system via exciton coupling over the double-strand with remaining relatively high fluorescence quanum yield.

Introduction

Naturally occurring double-stranded polymers, such as DNA and proteins, display exquisite molecular organization in biological systems. Double-stranded DNA is currently emerging as a passive scaffold and provides state-of-the-art bottom-up nanotechnology with molecular scale precision, as exemplified by DNA-origami.[1] This shape-programmable nanotechnology is enabled by both sequence-specific double-strand formation and the shape-persistent double-stranded building units. Therefore, the development of an intelligent double-strand as a building material for sophisticated hierarchical architectures in which to integrate functionality should be of significant interest. The present study examines novel double-strand-forming oligomeric porphyrin arrays that may, in a straightforward manner, be used to incorporate photoelectronic functions into structures for artificial photosynthesis.

The high fidelity of Watson–Crick base pairing via complementary hydrogen bonds plays a crucial role in the formation of double-stranded DNA.[2] In a similar way, artificial double-strands require the molecular design of complementary pairs through either multiple hydrogen bonds[3] or charge-transfer interactions.[4] Whereas the majority of research in the field has been devoted to the formation of helical structures,[5] almost no synthetic effort has been aimed at the applications of these structures in nanomaterials science, though they represent a promising new paradigm in bottom-up molecular assembly. The molecular design of supramolecular building materials could include not only sequence selectivity but also the shape-persistence of the functional double-stranded structures.

For decades, porphyrin frameworks have been part of technological advancements at the forefront of material studies because of their large π-systems and outstanding molar extinction coefficients. Their structural relevance in natural photosynthetic systems has been the source of considerable interest and has driven research in supramolecular multiporphyrin architectures.[6,7] The rigid porphyrin plane offers an ideal platform for versatile multiporphyrin architectures that can be built using both covalent and supramolecular approaches.[8,9] Biomimetic supramolecular porphyrin architectures with slipped-cofacially stacked conformations have been a useful motif for the design of materials with excellent photoelectronic functionalities, as described by Kobuke and coworkers.[10,11] A coordination-directed approach is particularly effective in the assembly of ladder complexes that are composed of fully π-conjugated multiporphyrin arrays via the use of bidentate ligands, as demonstrated by Anderson and collaborators.[12] The double-strand is an intriguing motif for use in creating a novel artificial photosynthetic system and engineering of discrete stacked π-system.

[a] *Faculty of Molecular Chemistry and Engineering, Kyoto Institute of Technology, Matsugasaki, Sakyo-ku, Kyoto 606-8585, Japan. E-mail address: morisue@kit.ac.jp; Fax: +81-75-724-7806.*

† Electronic Supplementary Information (ESI) available: Synthesis and full characterization of new compounds, electronic absorption spectra from titration experiments, and full characterization of $(\mathbf{1_1})_2$ and $(\mathbf{1_2})_2$ are described in the Supporting Information. See DOI: 10.1039/x0xx00000x

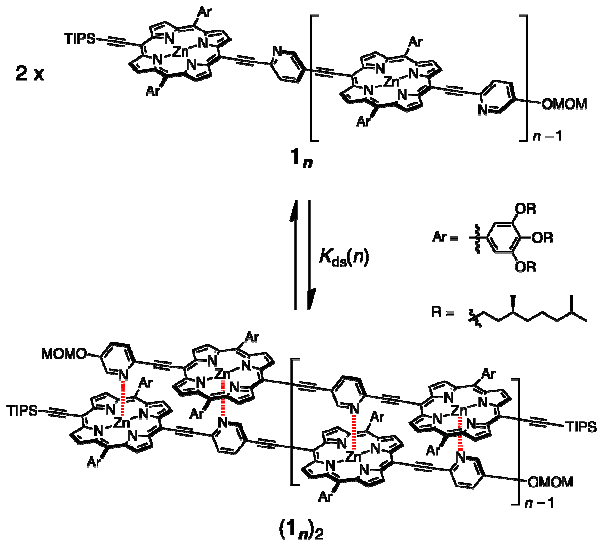

Scheme 1. Formation of double-strand $(\mathbf{1}_n)_2$ (n = 1–3).

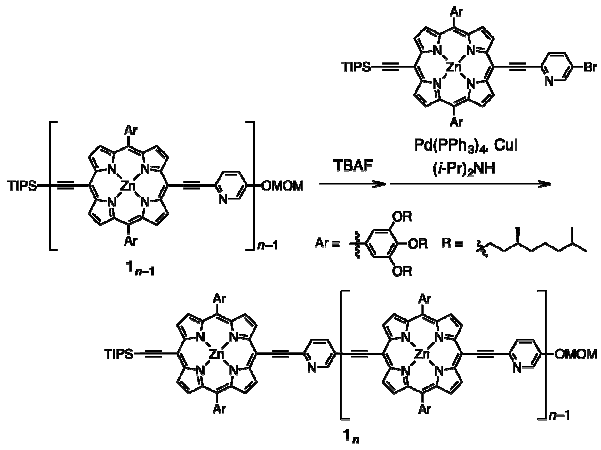

Scheme 2. Synthesis of porphyrin array $\mathbf{1}_n$ (n = 2–3).

In our previous report, the formation of self-coordinated zinc (2-pyridylethynyl)porphyrin dimers was controlled by the choice of the nucleation conditions, where the formation of the initial coordination bond governed how the second coordination bond formed.[13] In non-coordinating solvent, the formation of the second intra-dimer coordination bond was more energetically favorable to the initial binding was, which led to a self-complementary pattern of multiple coordination bonds. According to the same principle, we envisioned that oligomeric zinc (2-pyridylethynyl)porphyrin arrays $\mathbf{1}_n$ with an alternating pyridyl–porphyrin sequence could be assembled into a double-strand $(\mathbf{1}_n)_2$ (Scheme 1). The formation of the initial interstrand coordination bond would induce the spontaneous formation of the second and subsequent coordination bonds in a self-complementary fashion because of increasingly favorable thermodynamics of binding. This is the so-called zipper effect. Here, we present the molecular organization of novel double-stranded porphyrin arrays based on a self-complementary ligand–metalloporphyrin sequence, which provides successively stacked porphyrin arrays. The photophysical properties of these systems are studied.

Results and Discussion

Synthesis

The synthetic route to monomeric zinc (2-pyridylethynyl)porphyrin has already been established by our group.[13] According to the reported procedure, we prepared monomeric $\mathbf{1}_1$ as the precursor for oligomeric $\mathbf{1}_n$. A systematic series of new oligomers $\mathbf{1}_n$ (n = 2–3) were then prepared from $\mathbf{1}_1$ via repetitive Sonogashira–Hagihara coupling reactions (Scheme 2).[14] The details of the synthetic procedures are described in the Supporting Information, together with the essential thermodynamic and photophysical properties of $(\mathbf{1}_1)_2$ and $(\mathbf{1}_2)_2$. The following sections mainly demonstrate the results representative of $(\mathbf{1}_3)_2$, which is an assembly composed of six porphyrin rings and six pyridyl groups.

Structural Elucidation of Double-Strands

Double-strand $(\mathbf{1}_3)_2$ was observed using MALDI-TOF MS measurements (Figure 1A). $(\mathbf{1}_3)_2$ spontaneously formed as the lone stationary state in toluene, as identified by NMR. Only three sets of the protons in the pyridyl and porphyrin-β positions showed unambiguous diagonal correlations via the nuclear Overhauser effect (NOE) (Figure 1B), which is indicative of two trimeric porphyrin arrays that are cofacially assembled in an antiparallel arrangement (Figure 1A). The NOE correlation with the protons of the MOM group determined one of three porphyrin rings. Subsequently, the TOCSY correlations identified two sets of signals corresponding to the 2-, 3- and 6-pyridyl and 2′′-, 3′′- and 6′′-pyridyl protons. The alternating assignment for these two sets was also possible for these pyridyl–porphyrin pairs. However, these pyridyl protons individually showed NOE correlations with the porphyrin rings, which indicated pairing of the porphyrin rings with the complementary pyridyl groups. This finding is consistent with a symmetrically assembled structure, as indicated by a lack of multiplied signals of the porphyrin array. All of the aromatic resonances of the pyridyl groups were found in the non-aromatic region (6.34–2.56 ppm), which suggested that the axially coordinated pyridyl groups were strongly shielded in the vicinity of the porphyrin ring. The assignment is consistent with all of the observed NMR resonances.

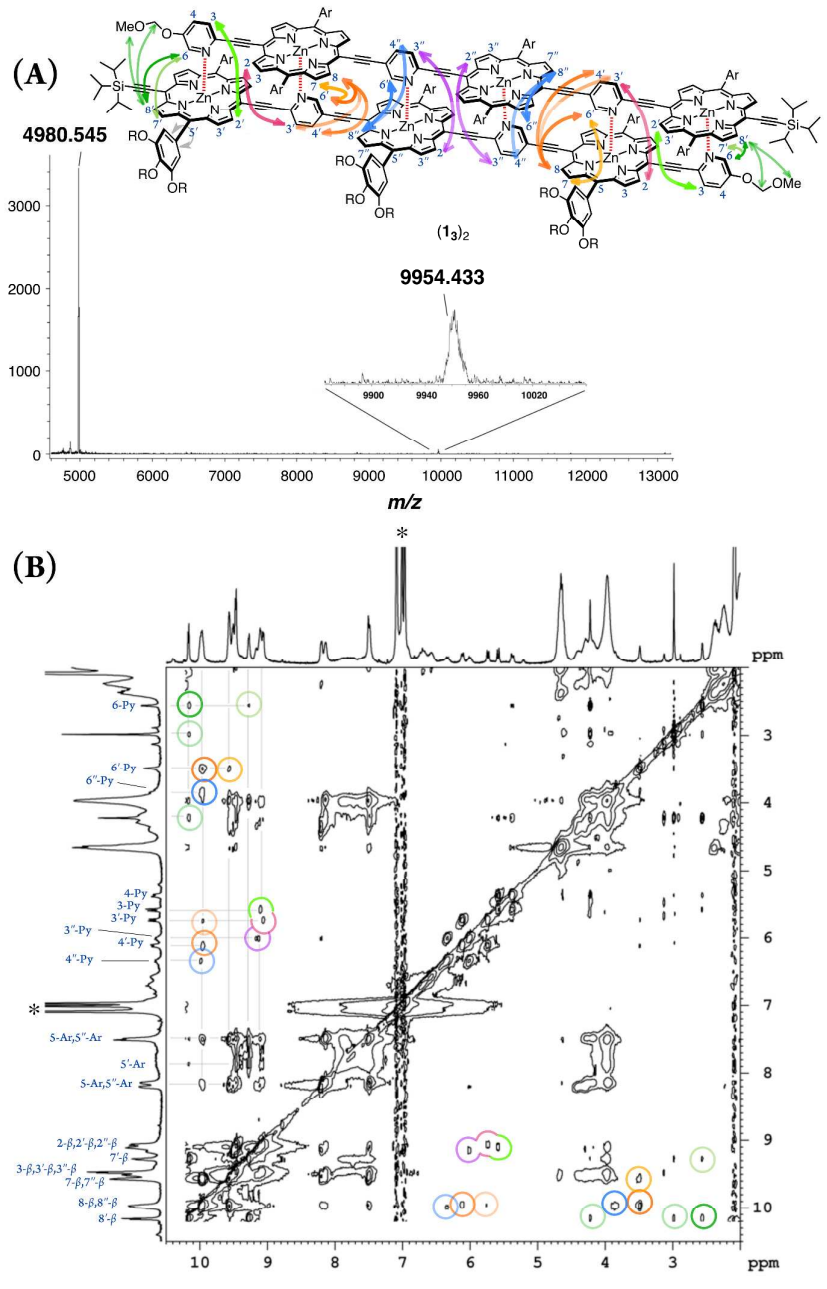

Figure 1. (A) MALDI-TOF MS spectrum of $(\mathbf{1_3})_2$. (B) ^{1}H–^{1}H NOE spectrum of $(\mathbf{1_3})_2$ in toluene-d_8. The asterisk indicates residual toluene. One alternative assignment is shown.

In pyridine-d_5, which can act as a competitively coordinating ligand, the non-shielded resonances of the pyridyl protons of the disassembled species were observed in the aromatic region with the disappearance of the upfield-signals observed for the double-strand. Comparison of the spectra in the two solvents suggests the assembly of the double-strand $(\mathbf{1_3})_2$ through pyridyl-to-zinc coordination bonds.[14] All of the NMR data firmly established the structural picture of a discrete double-strand $(\mathbf{1_3})_2$ assembled from an alternating pyridyl–porphyrin sequence via self-complementary coordination bonds.

Thermodynamic Behaviors

The double-strand $(\mathbf{1_3})_2$ was sufficiently durable enough to obey Beer's law over a wide concentration range (10^{-7}–10^{-4} M) in toluene. In contrast, the spectral shape of the electronic absorption spectra of $\mathbf{1_1}$ depended on the concentration, which suggested a small association constant for the formation of $(\mathbf{1_1})_2$ ($K_{ds}(1) = 1.3 \pm 0.2 \times 10^4$ M^{-1}).[14] The association constant of $(\mathbf{1_3})_2$, $K_{ds}(3)$, was found to be too high to directly evaluate the thermodynamic stability of the double-strand $(\mathbf{1_3})_2$. Over the course of competitive titration experiments with pyridine, the spectral changes showed several pseudo-isosbestic points, which suggested that the equilibria involved essentially two stationary states, *i.e.*, the double-strand and unzipped single-strand (Figure 2). Competitive titration experiments allowed us to analyze the thermodynamic stability of the double-strands according to the thermodynamic cycle (Scheme 3). We analyzed the unzipping equilibria by employing a tentative one-step unzipping model, which is useful for the description of the simplified overall equilibria. Nonlinear least-squares fittings gave reliable binding properties for the overall unzipping equilibria.[14] The overall unzipping constant (K_{uz}) is then described as follows;

$$K_{uz}(n) = \frac{[\mathbf{1}_n \cdot \mathrm{L}_n]^2}{[(\mathbf{1}_n)_2][\mathrm{L}]^{2n}} \quad (1)$$

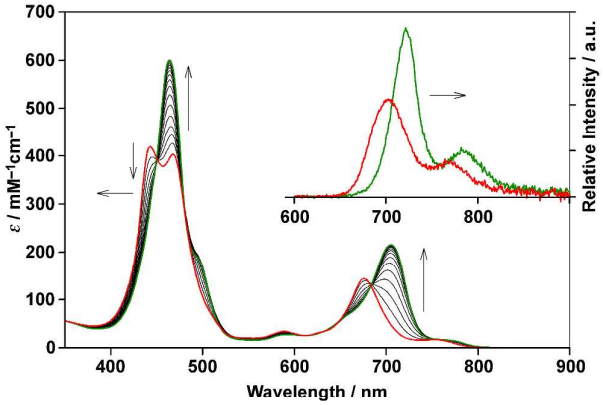

Figure 2. Spectrometric titration of $(\mathbf{1_3})_2$ ($[\mathbf{1_3}]_0 = 2.9 \times 10^{-6}$ M) with pyridine (up to 480 equiv., red to green) at 25 °C in toluene. The inset shows the fluorescence spectra of $(\mathbf{1_3})_2$ and $\mathbf{1_3}$ in the presence of excess pyridine (10^4 equiv.) in toluene (λ_{ex} = 450 nm, a pseudo-isosbestic point).

Assuming that the microscopic binding constant (K_μ) for the each ligand-to-zinc axial coordination bonds of the single-strand is identical, the microscopic binding constant can be approximated by equation 2.

$$K_\mu = \frac{[\mathbf{1}_n \cdot \mathrm{L}_n]^{1/n}}{[\mathbf{1}_n]^{1/n}[\mathrm{L}]} = \frac{[\mathbf{2}_{Si} \cdot \mathrm{L}]}{[\mathbf{2}_{Si}][\mathrm{L}]} \quad (2)$$

In practice, the titration of model zinc porphyrin $\mathbf{2_{Si}}$ with pyridine to yield axially coordinated zinc porphyrin gave the experimental K_μ values (K_μ = (3.2 ± 0.1) × 10^4 M^{-1}) (Scheme 3B). The values, in turn, gave the binding constant for double-strand formation ($K_{ds}(n)$) according to equation 3.

$$K_{ds}(n) = \frac{[(\mathbf{1}_n)_2]}{[\mathbf{1}_n]^2} = \frac{{K_\mu}^{2n}}{K_{uz}(n)} \quad (3)$$

These estimated thermodynamic parameters are useful in the discussion of the durability of the double-strand $(\mathbf{1_n})_2$ (Table 1). The values of $K_{ds}(n)$, $K_{ds}(2)$ = (2.5 ± 0.3) × 10^9 M^{-1} and $K_{ds}(3)$ = (6.5 ± 1.2) × 10^{11} M^{-1}, were remarkable, considering small magnitude of the microscopic binding constant as described below.

The zipper effect was quantified by the synergetic free energy change ($\Delta\Delta G(n)$), the excess energy beyond the sum of the independent free energy changes induced by pyridyl-to-zinc axial coordinating and π-stacked microscopic binding.[15]

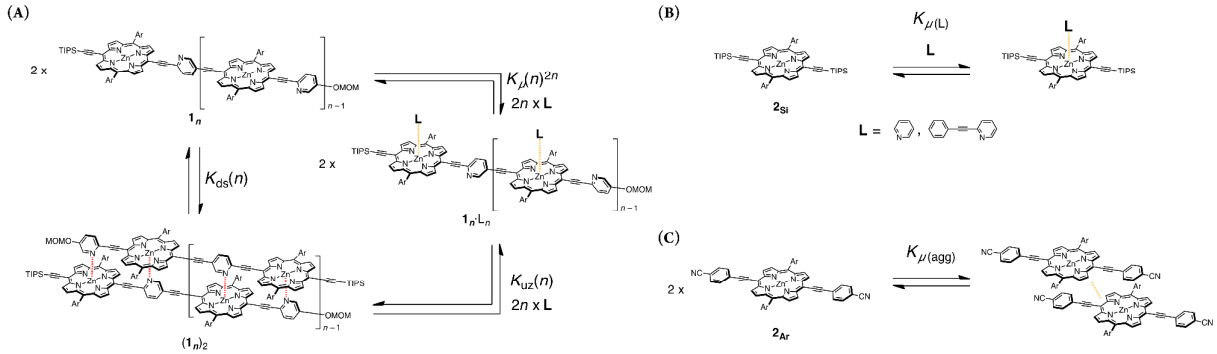

Scheme 3. (A) Generic closed thermodynamic cycle (n = 2–3). (B) Microscopic binding equilibrium of model porphyrin $\mathbf{2_{Si}}$ with axial ligands; L = pyridine and 2-(phenylethynyl)pyridine. (C) Aggregation equilibrium of model porphyrin $\mathbf{2_{Ar}}$.

Table 1. Thermodynamic parameters of $\mathbf{1}_n$ at 25 °C in Toluene.

	n	$K_{uz}(n)$ / M^{1-2n} [a]	$K_{ds}(n)$ / M^{-1} ($\Delta G_{ds}°(n)$ / kJ·mol^{-1})	$\Delta\Delta G°(n)$ / kJ·mol^{-1} [d] (EM / M) [e]
$\mathbf{1_1}$	1	–	(1.3 ± 0.2) × 10^4 (–23 ± 1) [b]	–12 ± 0.4 (147 ± 9)
$\mathbf{1_2}$	2	(4.1 ± 0.2) × 10^8	(2.5 ± 0.3) × 10^9 (–53 ± 1) [c]	–31 ± 0.2 (68 ± 8)
$\mathbf{1_3}$	3	(6.5 ± 1.2) × 10^{15}	(1.7 ± 0.3) × 10^{11} (–64 ± 1) [c]	–31 ± 0.2 (12 ± 1)

a) Estimated from the competitive titration experiments with pyridine. *b*) Directly estimated from variations in concentration. *c*) Estimated by Equation 3, wherein K_μ = (3.2 ± 0.1) × 10^4 M^{-1}. *d*) Estimated by employing $\Delta G_\mu°$ = –5.5 ± 0.3 kJ·mol^{-1}, wherein $K_\mu = {K_{\mu(L)}}^{1/2} \cdot {K_{\mu(agg)}}^{1/2}$ = 9.4 ± 1 M^{-1}. *e*) Effective molarity (EM) was evaluated from equation 6.

$$\Delta\Delta G(n) = \Delta G_{ds}(n) - 2n\Delta G_{\mu} \quad (4)$$

The $\Delta\Delta G(n)$ values substantially dominated the stability of the double-strands, with the multiple axial coordination bonds defining the discrete conformation of the double-strand despite their minimal thermodynamic contribution. To quantify a reliable microscopic binding constant, we employed model compounds. The binding constant for axial coordination of 2-(phenylethynyl)pyridine to $\mathbf{2_{Si}}$ as the model for the each ligand-to-zinc axial coordination bonds ($K_{\mu(L)}$ = 7.8 ± 1.1 M^{-1}, Scheme 3B) and that for self-aggregation of $\mathbf{2_{Ar}}$ as the model for π-stacked interaction ($K_{\mu(agg)}$ = 11 ± 1 M^{-1}, Scheme 3C). The microscopic binding constant for single coordination together with π-stacked interaction was, then, determined to be 9.4 ± 1 M^{-1} ($K_{\mu} = K_{\mu(L)}^{1/2} \cdot K_{\mu(agg)}^{1/2}$, ΔG_{μ}° = –5.5 ± 0.3 kJ·mol^{-1}). The dramatic change from $\Delta\Delta G^{\circ}(1)$ to $\Delta\Delta G^{\circ}(2)$ suggested that the zipper effects, a consequence of chelate cooperativity including such as π-stacking, van der Waals interactions, and desolvation entropy, became greater with addition of the repeating units. In contrast, the $\Delta\Delta G^{\circ}(3)$ value was similar to $\Delta\Delta G^{\circ}(2)$, which indicated that the compensatory effects gave rise to structural strain, such as distortion of the porphyrin planes, and loss of structural entropy. The analyses elucidated that the increasing number of the repeat units increased the durability of $(\mathbf{1}_n)_2$, although the cooperativity per interactions decreased. The nucleation step of the multiple coordination bonds is dominant for $\mathbf{1}_n$ self-assembles, and the synergetic effect governs the durability of $(\mathbf{1}_n)_2$ as long as n up to 3. The self-complementary coordination bonds were significantly stabilized by the zipper effect, thereby thermodynamically funnelling the self-assembled structures into the most stable form without kinetic entrapment by metastable states. This allowed for the realization of specific double-strand formation.

The situations are alternatively examined in term of "effective molarity (*EM*)", an empirical parameter to describe the effectiveness of the intramolecular interactions, to index the upper limit of the concentrations for the double-strand formation. The *EM* value is defined as equation 5 and 6.[16,17]

$$EM = (K_{ds}(n)/K_{\mu}^{2n})^{1/(2n-1)} \quad (5)$$

$$= \exp\{-\Delta\Delta G(n)/(2n-1)RT\} \quad (6)$$

The *EM* values of $(\mathbf{1_1})_2$ and $(\mathbf{1_2})_2$ (Table 1) were in high end range of typical values on supramolecular systems,[17] inferring that the model systems were, in the most precise sense, imperfect for the formation of the discrete double-strands. However, the *EM* values predicted significant selectivity of the double-strand formation even at very concentrated conditions.

Self-Sorting Behaviors

The exclusive formation of self-complementary double-strands $(\mathbf{1}_n)_2$ intrinsically involves self-sorting behaviors due to the possibility of several binding patterns for the self-association of $\mathbf{1}_n$ (Scheme 4). Briefly, *social* self-sorting favors self-complementary binding patterns, whereas *narcissistic* self-

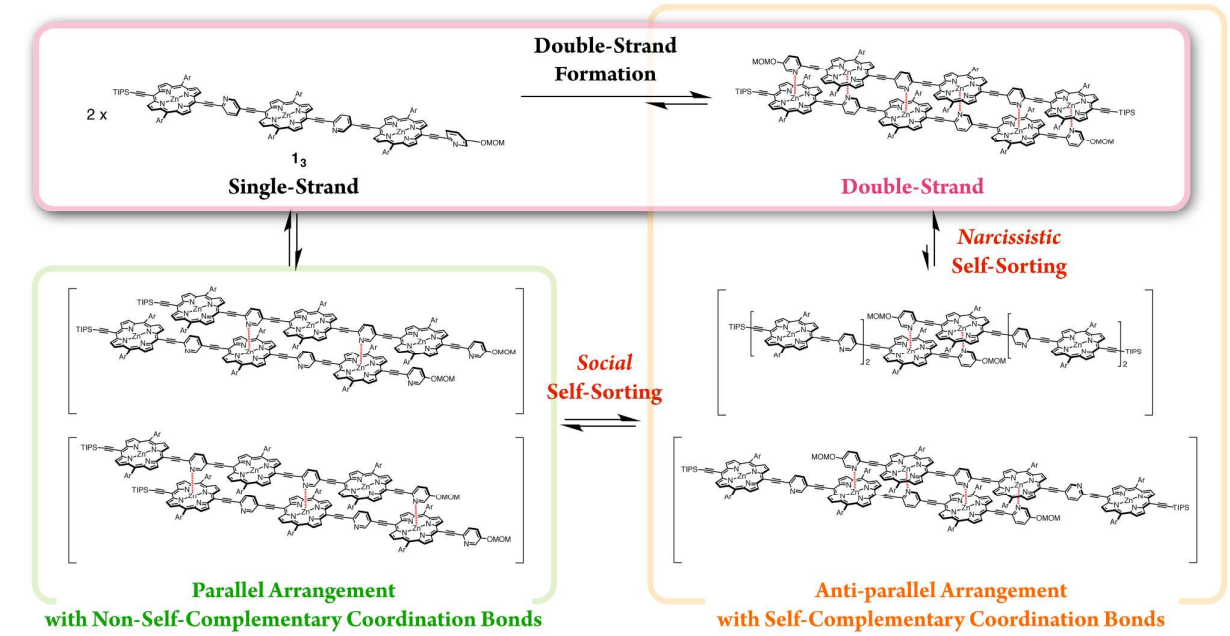

Scheme 4. Double-strand formation of $\mathbf{1_3}$ self-sorted from possible self-assembled patterns.

sorting distinguishes differences in the numbers of the repeating units of self-complementary binding patterns.[12b,18] Based on the lack of hysteresis, the self-sorting assembly of double-strands occurred during heating/cooling processes (25–70 °C) of a binary mixture of $(\mathbf{1_2})_2$ and $(\mathbf{1_3})_2$.[14] The electronic absorption spectra remained a superimposition of the spectra of $(\mathbf{1_2})_2$ and $(\mathbf{1_3})_2$ at 25 °C before and after heating, although thermally dissociated $\mathbf{1_2}$ and $\mathbf{1_3}$ mutually interacted to a degree at 70 °C. Mutually orthogonal self-assembly from a thermally unzipped mixture perfectly restored the initial fluorescence properties, indicated by the superimposition of $(\mathbf{1_2})_2$ and $(\mathbf{1_3})_2$ at 25 °C. The self-sorting capacity of the double-strands $(\mathbf{1}_n)_2$ makes them promising in the construction of units that are capable of simultaneous multiple molecular assembly within bottom-up nanotechnology applications.

Engineering Discrete Stacked π-System

In the last stage, our attention turned to the electronic properties of the double-strands $(\mathbf{1_2})_2$ and $(\mathbf{1_3})_2$. The double-strand formation of $\mathbf{1}_n$ resulted in a successively slipped-cofacial stack of porphyrin arrays. The double-strands $(\mathbf{1}_n)_2$ showed splitting of the Soret band with a bathochromic shift of the lower band due to exciton coupling in the electronic absorption spectra.[10,19] The split width of the Soret band of $(\mathbf{1_3})_2$ (0.14 eV) was wider than that of $(\mathbf{1_2})_2$ (0.10 eV), where the lower exciton band was red-shifted and the higher exciton band remained unchanged. At the same time, the Q band of $(\mathbf{1_3})_2$ displayed a larger bathochromic shift to 675 nm (1.83 eV) than that of $(\mathbf{1_2})_2$ at 669 nm (1.85 eV), where the longest Zn···Zn distances were estimated to be 43 Å for $(\mathbf{1_3})_2$ and 25 Å for $(\mathbf{1_2})_2$ based on the geometry-optimized structures (Figure 3). Comparison of the electronic structures of $(\mathbf{1_3})_2$ and $(\mathbf{1_2})_2$ unveiled that the double-stranded multiporphyrin array exhibited exciton coupling due to the successive slipped-cofacial stacks, leading to long-range π-electronic interactions.

The emission properties are noteworthy because the double-strands $(\mathbf{1}_n)_2$ did not dissipate a photoexcited singlet. The absolute fluorescence quantum yields (Φ) of $(\mathbf{1_2})_2$ and of $(\mathbf{1_3})_2$ were 0.15 and 0.20, respectively (Table 2). Increasing the number of the porphyrin units raised the Φ values through extending the π-systems. The relatively high fluorescence efficiency of $(\mathbf{1}_n)_2$ suggested that the double-stranded structure was effective in circumventing nonradiative deactivation pathways, even in the near-infrared wavelength region. The successive slipped-cofacial stacks of the porphyrin planes in the double-strand serve as structural and functional mimics of bacterial light-harvesting antenna complexes that display efficient capture of sunlight and photoexcited energy transfer.[7]

Table 2. Photophysical properties of double-strand $(\mathbf{1}_n)_2$, $\mathbf{1}_n$ accommodated with Pyridine ($\mathbf{1}_n$·Py$_n$) and **2** in Toluene.

	λ_{em} / nm (Φ) [a)]	τ / ns (α)	k_{em} / s^{-1} [e)]
$(\mathbf{1_2})_2$	690 (0.15)	0.65 (0.51), 1.15 (0.49) [b)]	1.7×10^8
$(\mathbf{1_3})_2$	702 (0.20)	0.56 (0.32), 1.03 (0.68) [b)]	2.3×10^8
$\mathbf{2_{Si}}$	635 (0.07)	1.61 [c)]	4.3×10^7
$\mathbf{2_{Si}}$·Py	650 (0.08)	1.45 [d)]	5.6×10^7

a) Emission maximum (λ_{em}) and fluorescence quantum yield (Φ) obtained using an integration sphere (excitation by 452 nm for $(\mathbf{1_2})_2$, 450 nm for $(\mathbf{1_3})_2$, and 405 nm for $\mathbf{2_{Si}}$ and $\mathbf{2_{Si}}$·Py). *b*) Fluorescence lifetime (τ) and the normalized amplitude (α) determined from the fluorescence decay profiles in the range of 623–773 nm upon excitation at 483 nm (Figure 5). *c*) Emission at 635 nm upon excitation by 405 nm. *d*) Emission at 650 nm upon excitation by 405 nm. *e*) Radiative rate constant defined as $k_{em} = \Phi/\tau$. The single-strand $\mathbf{2_{Si}}$·Py was observed in the presence of excess pyridine (10^4 equiv.).

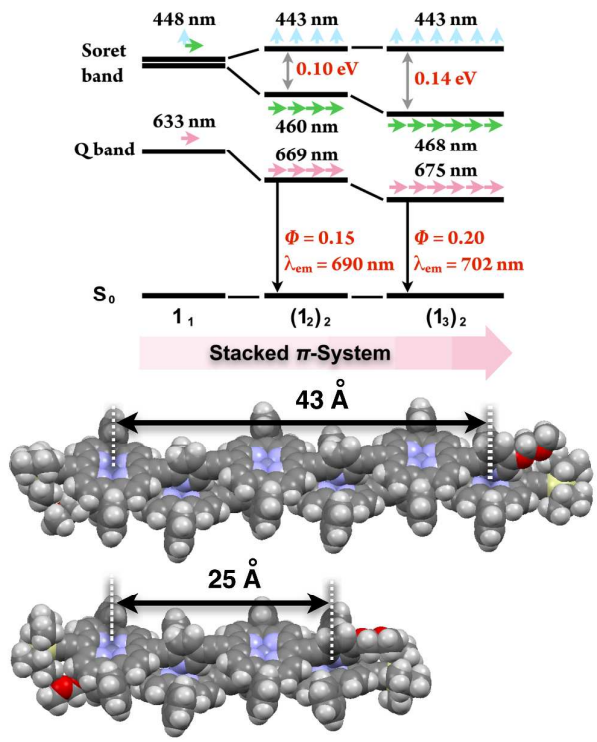

Figure 3. Energy diagrams of double-strand $(\mathbf{1}_n)_2$, and their geometry-optimized structures calculated using the MM+ force field (HyperChem Ver. 8.0 software). The alkoxy side chains are omitted for visual clarity. The wavelengths denote the absorption maxima.

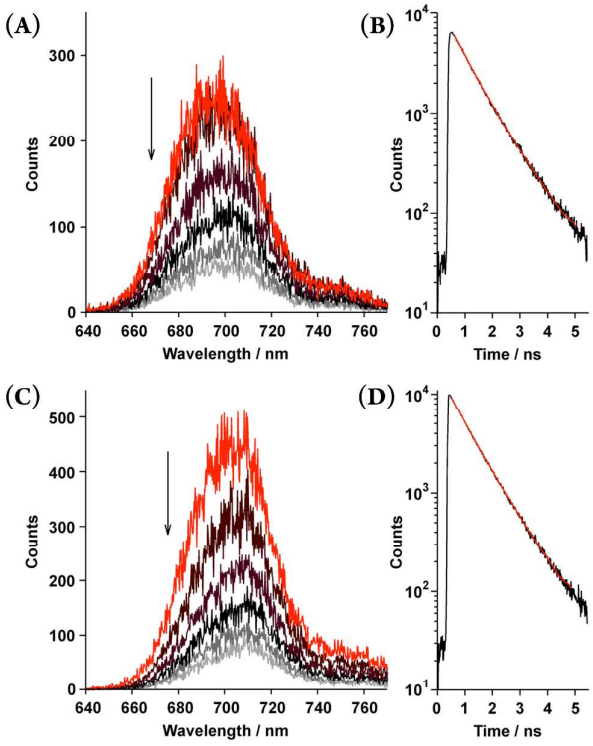

Figure 4. Time-resolved fluorescence spectra recorded every 0.3 ns (upper to lower; 0.45–0.55, 0.75–0.85, 1.05–1.15, 1.35–1.45, 1.65–1.75, and 1.95–2.05 ns) and the fluorescence decay profiles of the double-strands $(\mathbf{1_2})_2$ at $[\mathbf{1_2}] = 5.5 \times 10^{-6}$ M (A, B) and $(\mathbf{1_3})_2$ at $[\mathbf{1_3}] = 6.9 \times 10^{-6}$ M (C, D) in toluene. The fluorescence decay profiles (black line) are shown with fitted curves based on biexponential decay constants (red line, τ shown in Table 2) in the range of 623–773 nm.

Time-resolved fluorescence spectroscopy gave further insight into the photophysical dynamics of the excited-states (Figure 4). The biexponential fluorescence decay profiles of both double-strands indicated the existence of dual fluorescent states (Table 2). Over time, the double-strand $(\mathbf{1_3})_2$ showed a small red-shift in its emission wavelength. In contrast, the spectral shift of $(\mathbf{1_2})_2$ was smaller than that of $(\mathbf{1_3})_2$. It is intriguing to consider that the photophysical properties have relevance to the thermodynamic aspect of the double-strands; $(\mathbf{1_3})_2$ was much strained than $(\mathbf{1_2})_2$. The structural relaxation could provide an energy sink that is capable to trapping photoexcited singlets. For instance, it is known that the porphyrin plane is ruffled in the photoexcited singlet state.[20,21] This interpretation is the likely reason why the slower fluorescence decay manifests by red-shift.

Conclusions

In summary, we have synthesized double-stranded porphyrin arrays that yield successive slipped-cofacial stacks with strong exciton coupling. Titration experiments revealed the thermodynamic aspects underlying the specific double-strand formation, which are used to describe a process in which self-complementary coordination bonds defined the discrete structure and the zipper effect dominated the stability of the double-stranded structure. The remarkable selectivity of the double-strand formation may serve as a powerful building tool for sophisticated bottom-up molecular assemblies with molecular scale precision, similar to those found in DNA nanotechnology. Moreover, the double-strands extended the π-electron network without any dissipation of the fluorescence properties due to the successive slipped-cofacial stack assembly. The shape-persistent double-stranded porphyrin arrays provide new options for artificial photosynthetic systems based on shape-programmable, bottom-up molecular architectures.

Acknowledgements

This work was partly supported by a Grant-in-Aid for Scientific Research (No. 25102525) on the Innovative Area “New Polymeric Materials Based on Element-Blocks (No. 2401)” from the Ministry of Education, Culture, Sports, Science and Technology, Government of Japan. The authors thank Prof. Shinjiro Machida (Kyoto Institute of Technology) for time-resolved fluorescence spectroscopy. We thank the referees for their helpful suggestions for thermodynamic analyses.

Notes and references

1 DNA nanotechnology: (*a*) P. W. K. Rothemund, *Nature* 2006, **440**, 297–302; (*b*) F. A. Aldaye, A. L. Palmer, H. F. Sleiman, *Science* 2008, **321**, 1795–1799; (*c*) M. S. Strano, *Science* 2012, **338**, 890–891; (*d*) B. Sacca, C. M. Niemeyer, *Angew. Chem. Int. Ed*. 2012, **51**, 58–66; (*e*) A. Rajendran, M. Endo, H. Sugiyama, *Angew. Chem. Int. Ed*. 2012, **51**, 874–890; (*f*) F. Zhang, J. Nangreave, Y. Liu, H. Yan, *J. Am. Chem. Soc.* 2014, **136**, 11198–11211; (*g*) M. R. Jones, N. C. Seeman, C. A. Mirkin, *Science* 2015, **347**, 1260901.

2 (*a*) W. Saenger, *Principle of Nuceic Acid Structure*, Springer–Verlag: New York (1984); (*b*) J. SantaLucia, Jr. H. T. Allawi, P. A. Seneviratne, *Biochemistry* 1996, **35**, 3555–3562.

3 Hydrogen-bonding: (*a*) A. P. Bisson, F. J. Carver, C. A. Hunter, J. P. Waltho, *J. Am. Chem. Soc*. 1994, **116**, 10292–10293; (*b*) A. P. Bisson, F. J. Carver, D. S. Eggleston, R. C. Haltiwanger, C. A. Hunter, D. L. Livingstone, J. F. McCabe, C. Rotger, A. E. Rowan, *J. Am. Chem. Soc*. 2000, **122**, 8856–8868; (*c*) V. Berl, I. Huc, R. G. Khoury, M. J. Krische, J.-M. Lehn, *Nature*, 2000, **407**, 720–723; (*d*) T. Maeda, Y. Furusho, S.-i. Sakurai, J. Kumaki, E. Yashima, *J. Am. Chem. Soc.* 2008, **130**, 7938–7945; (*e*) H. Goto, Y. Furusho, K. Miwa, E. Yashima, *J. Am. Chem. Soc*. 2009, **131**, 4710–4719; (*f*) H. Yamada, Z.-Q. Wu, Y. Furusho, E. Yashima, *J. Am. Chem. Soc.* 2012, **134**, 9506–9520.

4 Charge-transfer interactions: (*a*) G. J. Gabriel, B. L. Iverson, *J. Am. Chem. Soc*. 2002, **124**, 15174–15175; (*b*) Q.-Z. Zhou, X.-K. Jiang, X.-B. Shao, G.-J. Chen, M.-X. Jia, Z.-T. Li, *Org. Lett*. 2003, **5**, 1955–1958; (c) Q.-Z. Zhou, QM.-X. Jia, X.-B. Shao, L.-Z. Wu, X.-K. Jiang, Z.-T. Li, G.-J. Chen, *Tetrahedron* 2005, **61**, 7117–7124.

5 Reviews: (*a*) D. Haldar, C. Schmuck, *Chem. Soc. Rev*. 2009, **38**, 363–371; (*b*) Y. Furusho, E. Yashima, *Macromol. Rapid*

Commun. 2011, **32**, 136–146, and the references cited therein.
6 (*a*) G. McDermott, S. M. Prince, A. A. Freer, A. M. Hawthornthwaite-Lawless, M. Z. Papiz, R. J. Cogdell, N. W. Isaacs, *Nature* 1995, **374**, 517–521; (*b*) A. W. Roszak, T. D. Howard, J. Southall, A. T. Gardiner, C. J. Law, N. W. Isaacs, R. J. Cogdell, *Science* 2003, **302**, 1969–1972; (*c*) S. Niwa, L.-J. Yu, K. Takeda, Y. Hirao, T. Kawakami, Z.-Y. Wang-Otomo, K. Miki, *Nature* 2014, **508**, 228–232.
7 (*a*) R. J. Cogdell, A. Gall, J. Köhler, *Q. Rev. Biophys*. 2006, **39**, 227–324; (*b*) V. Sundström, *Annu. Rev. Phys. Chem*. 2008, **59**, 53–77.
8 Covalent multiporphyrin architectures: (*a*) A. K. Burrell, D. L. Officer, P. G. Plieger, D. C. W. Reid, *Chem. Rev*. 2001, **101**, 2751–2796; (*b*) D. Kim, A. Osuka, *Acc. Chem. Res*. 2004, **37**, 735–745; (c) N. Aratani, A. Osuka, *in Handbook of Porphyrin Science*; K. M. Kadish, K. M. Smith, R. Guilard, Eds.; World Scientific: Singapore, Vol. 1, Chapter 1 (2010).
9 Supramolecular multiporphyrin architectures: (*a*) J. Wojaczynski, L. Latos-Grazynski, *Coord. Chem. Rev*. 2000, **204**, 113–171; (*b*) I. Beletskaya, V. S. Tyurin, VA. Y. Tsivadze, R. Guilard, C. Stern, *Chem. Rev.* 2009, **109**, 1659–1713; (c) J. S. A. W. Elemans, R. van Hameren, R. J. M. Nolte, A. E. Rowan, *Adv. Mater*. 2006, **18**, 1251–1266; (d) C. Zou, C.-D. Wu, *Dalton Trans*. 2012, **41**, 3879–3888; (e) S. Durot, J. Taesch, V. Heitz, *Chem. Rev*. 2014, **114**, 8542–8578.
10 M. Morisue, Y. Kobuke, *in Handbook of Porphyrin Science*; Kadish, K. M.; Smith, K. M.; Guilard, R. Eds.; World Scientific: Singapore, Vol. 32, Chapter 166 (2014).
11 (*a*) Y. Kobuke, H. Miyaji, *J. Am. Chem. Soc*. 1994, **116**, 4111–4112; (*b*) K. Kameyama, M. Morisue, A. Satake, Y. Kobuke, *Angew. Chem. Int. Ed*. 2005, **44**, 4763–4766; (*c*) M. Morisue, Y. Kobuke, *Chem.–Eur. J*. 2008, **14**, 4993–5000.
12 (*a*) H. L. Anderson, *Inorg. Chem*. 1994, **33**, 972–981; (*b*) P. N. Taylor, H. L. Anderson, *J. Am. Chem. Soc*. 1999, **121**, 11538–11545; (*c*) J. K. Sprafke, B. Odell, T. D. W. Claridge, H. L. Anderson, *Angew. Chem. Int. Ed*. 2011, **50**, 5572–5575.
13 M. Morisue, T. Morita, Y. Kuroda, *Org. Biomol. Chem*. 2010, **8**, 3457–3463.
14 See the Supporting Information.
15 (*a*) S. L. Cockroft, C. A. Hunter, *Chem. Soc. Rev*. 2007, **36**, 172–188; (*b*) A. Camara-Campos, D. Musumeci, C. Hunter, S. Turega, *J. Am. Chem. Soc*. 2009, **131**, 18518–18524; (*c*) H. J. Hogben, J. K. Sprafke, M. Hoffmann, M. Pawlicki, H. L. Anderson, *J. Am. Chem. Soc*. 2011, **133**, 20962–20969.
16 (*a*) C. Galli, L. Mandolini, *Eur. J. Org. Chem*. 2000, 3117–3125; (*b*) A. Mulder, J. Huskens, D. N. Reinhoudt, *Org. Biomol. Chem.* 2004, **2**, 3409–3424; (*c*) C. A. Hunter, H. L. Anderson, *Angew. Chem. Int. Ed*. 2009, **48**, 7488–7499.
17 M. C. Misuraca, T. Grecu, Z. Freixa, V. Garanini, C. A. Hunter, P. W. N. M. van Leeuwen, M. D. Segarra-Maset, S. M. Turega, *J. Org. Chem*. 2011, **76**, 2723–2732.
18 (*a*) A. Wu, L. Isaacs, *J. Am. Chem. Soc*. 2003, **125**, 4831–4835; (*b*) M. M. Safont-Sempere, G. Fernández, F. Würthner, *Chem. Rev*. 2011, **111**, 5784–5814.
19 (*a*) M. Kasha, *Radiat. Res*. 1963, **20**, 55–71; (*b*) M. Kasha, H. R. Rawls, M. A. El-Bayoumi, *Pure Appl. Chem*. 1965, **11**, 371–392.
20 S. Gentemann, N. Y. Nelson, L. Jaquinod, D. J. Nurco, S. H. Leung, C. J. Medforth, K. M. Smith, J. Fajer, D. Holten, *J. Phys. Chem. B* 1997, **101**, 1247–1254.
21 (*a*) R. A. Freitag, J. A. Mercer-Smith, D. G. Whitten, *J. Am. Chem. Soc.* 1981, **103**, 1226–1228; (*b*) R. A. Freitag, D. G. Whitten, *J. Phys. Chem.* 1983, **87**, 3918–3925; (*c*) K. Konishi, K. Miyazaki, T. Aida, S. Inoue, *J. Am. Chem. Soc*. 1990, **112**, 5639–5640.

A table of contents entry

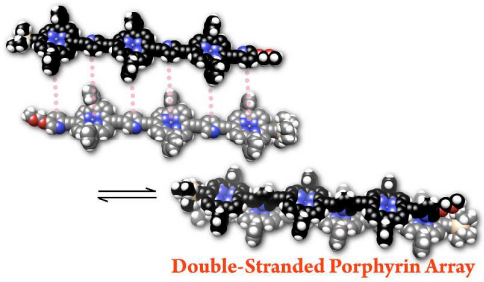

Double-Stranded Porphyrin Array